Chapter 6

Multifunction Multimode Power Processor Enabling IM drive with Auxiliary Power supplies for High Power EVs

6.1 Introduction

In this chapter, the design of a multifunction multimode power processor enabling induction motor (IM) drive with auxiliary power supplies for high-power EVs is presented. The on-board power processor enables vehicle-to-grid (V2G) power supply, vehicle-to-vehicle (V2V) charging, and induction motor (IM) drive operation, along with auxiliary power supply in the EV's cabin. Switching between different operating states is a crucial step in multifunction operation. Generally, relays are used as additional switches for the selection of the function, affecting the durability of the converter. In the newly proposed power processor, the functions are selected by the control logic in the microcontroller. The circuit diagram of the proposed power processor is given in Fig.6. 1. Further, the operation of the power processor can be understood by the flowchart as shown in Fig.6. 2.

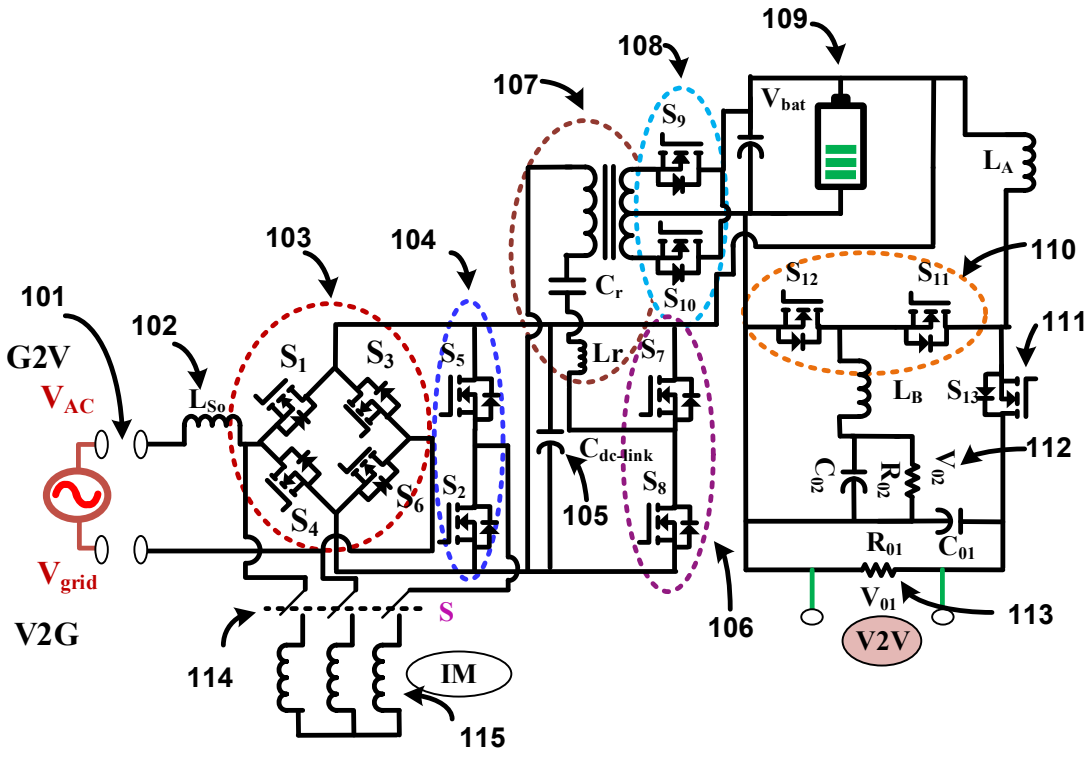

Fig.6. 1 Circuit diagram of the proposed power processor.

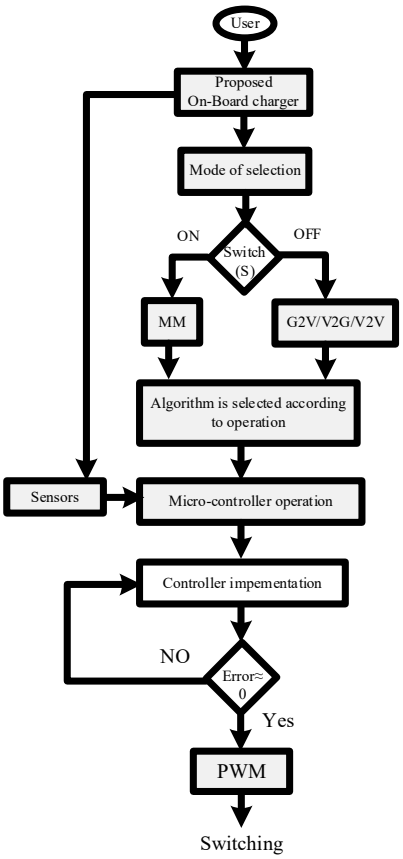

Fig.6. 2 Flowchart for the operation of the proposed power processor.

6.2 Selection of the function and its operation

The appearance of the proposed power processor in different functions and its operation are depicted in the flowchart. The function is selected by a single switch, "S". If the switch is ON, it performs motoring mode, and when it is OFF, it performs G2V, V2G, and V2V operations according to the function selection. After the selection of the function, the microcontroller activates the control algorithm. For these operations, all the sensing parameters are attached to the microcontroller. The control algorithm reduces the steady-state error to zero and generates the PWM according to the selected function. The operation of the proposed power processor is as follows

6.2.1 Single-phase (G2V) charging

In the proposed power processor 120V, a 50 Hz power supply is connected at the front end (101), and switch S (114) remains turned off, as shown in Fig.6. 3. The source inductor Lso (102) and switches S_1, S_4, S_3, and S_6 (103) charge the DC-link capacitor (105), the same as the AC/DC converter. During the single-phase charging operation,

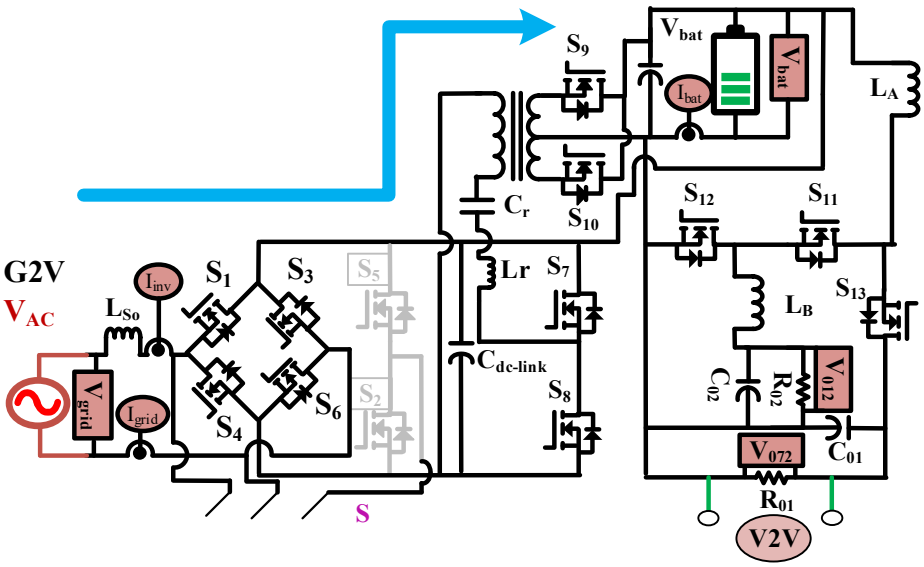

Fig.6. 3 Circuit diagram of the proposed power processor in single-phase charging.

the switches S_5 and S_2 (104) remain off. Switches S_7 and S_8 (106), resonant tank (107), and full wave rectifier S_9 and S_{10} (107) charge the battery (109) the same as the DC/DC converter. The whole process maintains the unity power factor at the source terminal and charges the battery with a constant-current constant-voltage (CC-CV) charging technique. At the same time, switches S_{11}, S_{12}, and S_{13} (110 and 111) with some passive components (L_A, L_B, C_{01}, C_{02}) generate two regulated outputs (112 and 113) from the AC supply source to cater to the power demand of the EV cabin.

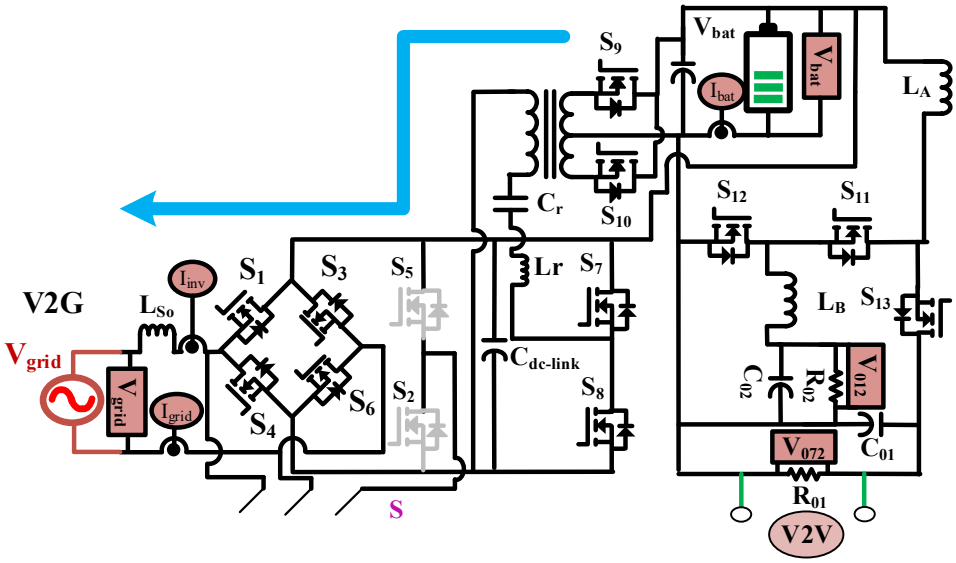

Fig.6. 4 Circuit diagram of the proposed power processor in V2G operation.

6.2.2 Vehicle-to-grid power supply

In the V2G power supply, the battery voltage is stepped up with the help of the switches S_9 and S_{10} (108), and the transformer is set up to charge the DC-link capacitor (105). Switches S_7, S_8, S_5, and S_2 (106 and 104) remain off. The stored energy in the DC-link capacitor is fed into the grid by synchronizing the inverter voltage with the grid voltage by switches S_1, S_4, S_3, and S_6 (103), as shown in Fig.6. 4. The auxiliary power supply takes the energy from the battery (109) with the help of the switches S_{11}, S_{12}, and S_{13} (110 and 111), the same as in charging mode.

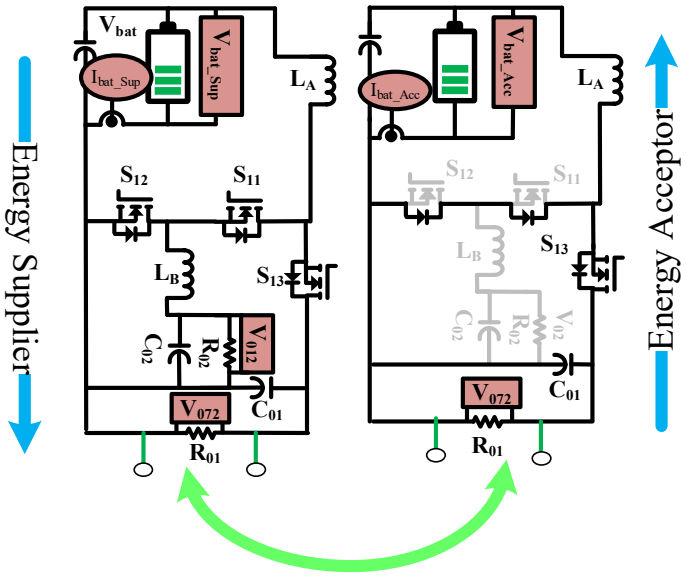

Fig.6. 5 Circuit connection of the proposed power processor during V2V charging.

6.2.3 Vehicle-to-vehicle charging

For V2V charging, the proposed power processor from both vehicles is connected, and the energy is exchanged with the help of six active switches, as shown in Fig.6. 5. The power processor from both vehicles is connected to the high-power auxiliary terminal (113).

6.2.4 Motoring mode operation

In motoring mode, switch S is turned ON, and the front end (101) remains open, as shown in Fig.6. 6. The proposed power processor takes power from the battery (109) and charges the DC-link capacitor (105) in the same way as the V2G power supply process. Switches S_1, S_2, S_3, S_4, S_5, and S_6 (103 and 104) are used to drive the motor (115) from the stored energy of the DC link capacitor (105) with the help of the respective control techniques.

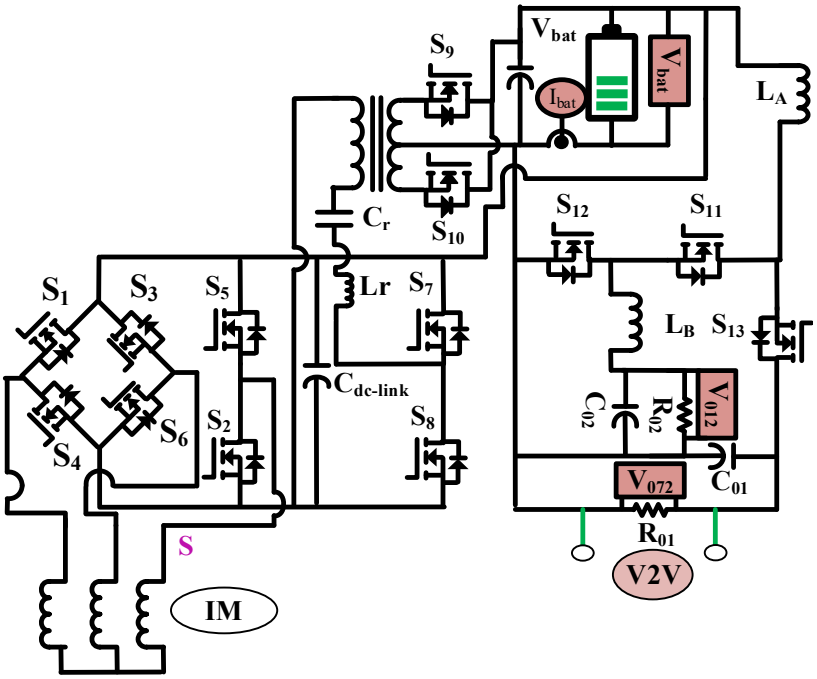

Fig.6. 6 Circuit diagram of the proposed converter in motoring mode.

6.3 Control operation of the proposed power processor

In multifunction operation, the control logic is very important to ensure the smooth operation of the power processor. Nine sensing parameters are used to implement these functions. 1) Input voltage/grid voltage (V_{in}, V_{grid}), 2) input current/ injected current (i_{in}/i_{inject}), 3) i_{grid}, 4) V_{bat} , 5) I_{bat} ,6) V_{01}, 7) I_{01}, 8) $I_{bet-accp}$, 9) $V_{bat-accp.}$ The rated power of the proposed power processor is given in Table 6. 1.

Table 6. 1 Operation of the proposed power processor at its rated value

Mode of operation	**Power IN**	**Voltage and Current rating at the load**			**Output Power (Watts)**
Charging	V_{in}= 120 V, I_{in} = 6.5 A	V_{bat}= 48V, I_{bat} = 5.5 A	V_{01}=72 V, I_{01} =5.5 A	V_{02}=12 V, I_{02} = 5A	264+396+60 = 720
Motoring	V_{bat} = 48 V I_{bat} = 16 A	V_{IM}=110V, I_{IM}= 2.4A	V_{01}=72 V, I_{01} =5.5 A	V_{02}=12V, I_{02} = 5 A	480+396+60 =720
V2V	V_{bat} = 48 V I_{bat} = 10 A	---	V_{01}=72 V, I_{01} =5.5 A	V_{02}=12V, I_{02} = 5 A	396+60= 456
V2G	V_{bat} = 48 V I_{bat} = 22A	V_{AC}=120 V Iac = 4.2 A	V_{01}=72 V, I_{01} =5.5 A	V_{02}=12V, I_{02} = 5 A	480+396+60=960
V_{bat} and I_{bat} (battery voltage and current), V_{01} and I_{01} (High-power auxiliaries' voltage and current), V_{02} and I_{02} (Low-Power auxiliaries' voltage and current), V_{IM} and I_{IM} (motor voltage and current rating), Vac= grid voltage, Iac= injected grid current					

6.3.1 Single-phase charging operation

Six sensing parameters, V_{in}, I_{in}, V_{bat}, I_{bat}, $V_{01,}$ and $V_{02,}$ are used to implement the single-phase charging, as shown in Fig.6. 7 (a) and (b). The proposed power processor maintains the

unity power factor at the source terminal and charges the battery with the CC-CV charging technique, through the control logic given in Fig.6. 7 (a). The tuning parameters of this control logic are determined by the $\frac{\hat{v}_{bat}}{\hat{i}_{in}}$ and $\frac{\hat{i}_{in}}{d_1}$ transfer function by the small signal analysis of the proposed power processor. During this operation, the regulated auxiliary power supplies are maintained through the control logic given in Fig.6. 7(b). The tuning parameter for this control logic is determined by the $\frac{V_{01}}{d_{01}}$ and $\frac{V_{02}}{d_{02}}$ transfer functions through the small signal analysis of the proposed converter.

6.3.2 Speed control of the induction motor

The speed of the induction motor is controlled by a variable frequency drive (VFD). In this method, the speed is controlled by varying the frequency of the power supply of the stator, as shown in Fig.6. 7(c). The frequency of the switches S_1, S_2, S_3, S_4, S_5, and S_6 varies in the revolving field of the stator, which indirectly controls the speed of the motor. Further, during the motor drive, the regulated auxiliary power supplies are controlled in the same way as in the charging operation, as shown in Fig.6. 7(b).

6.3.3 V2G power supply

Seven sensing parameters are used for the V2G operation, and those parameters are v_{grid}, i_{grid} , $i_{inv,}$ V_{bat} , I_{bat}, V_{01}, and V_{02}. The control logic for the V2G operation is shown in Fig.6. 7(d) During V2G operation, grid synchronization is very important, and this is achieved by the phase lock loop (PLL), as explained in Fig.6. 8. The two low-pass filters provide a phase delay of 90^0 for α and β parameters in the inverter output voltage, and the gain is compensated by a multiplying factor of 2. Further, the α, β to d, q transform is applied, and the V_q parameter is used for finding the phase synchronizing angle (Θ_{sc}), where f_g is the power frequency of the grid.

The desired injected current (i_{inj}) synchronizes with the grid with the help of the PLL and is controlled by the proportional-resonant (PR) controller. The equation of the PR controller is given in Eq. 6.1.

$$H_{AC}(s) = K_p + \frac{2K_i S}{S^2 + {w_o}^2} \tag{6.1}$$

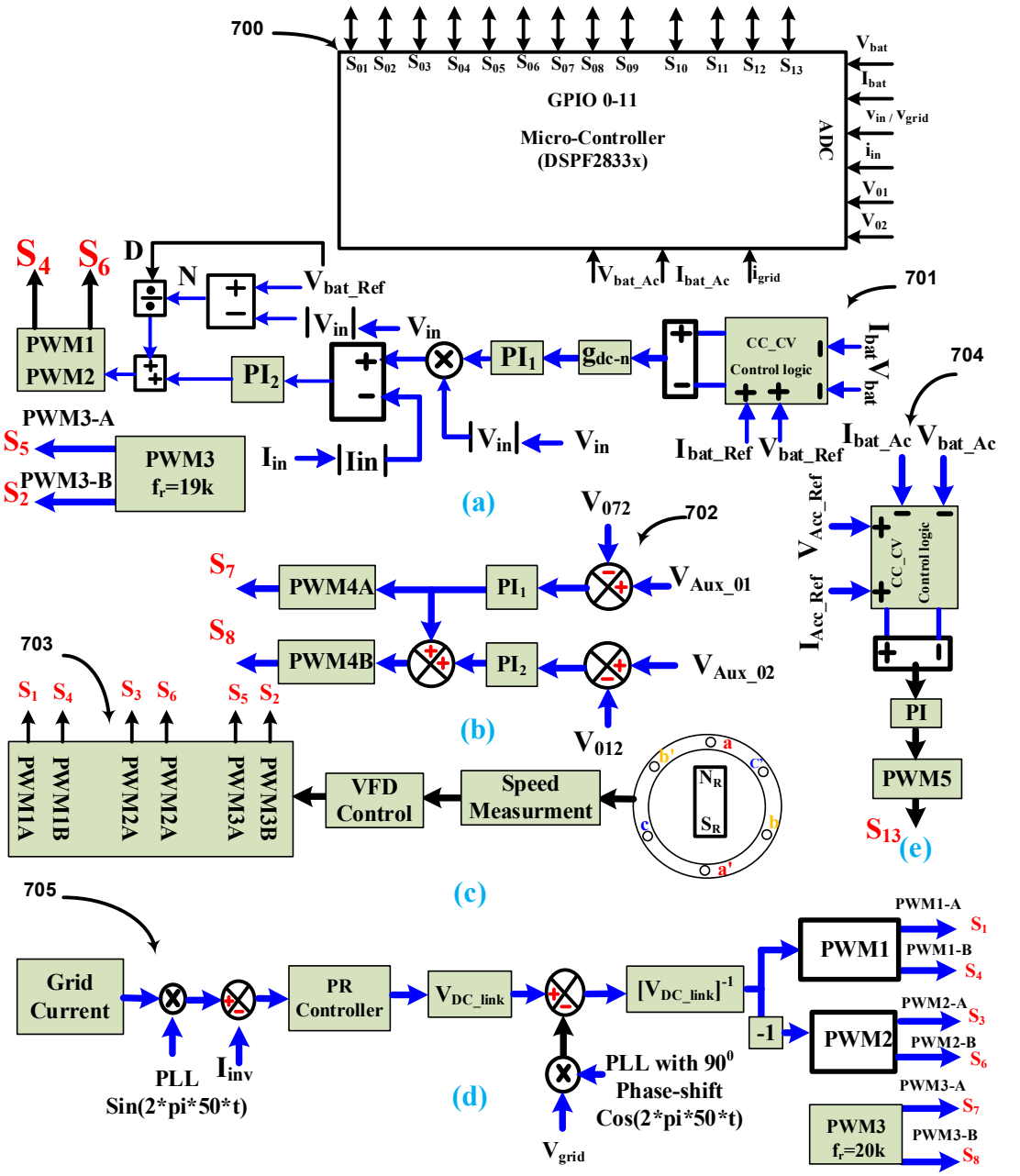

Fig.6. 7 Control logic of the proposed power processor.

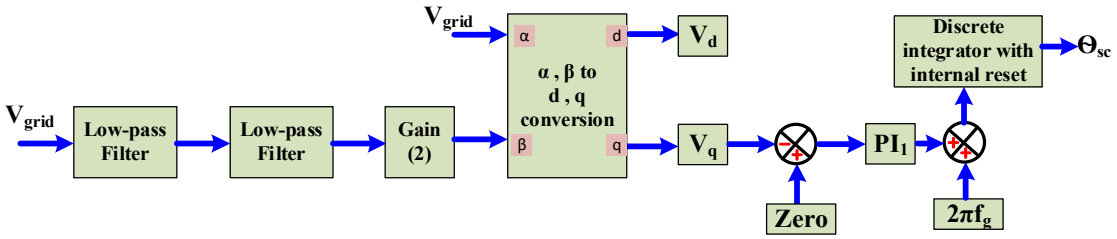

Fig.6. 8 Phase lock-loop for synchronizing angle.

Where $K_p = \frac{\alpha\sqrt{\alpha}\,\omega_0 L - r}{V_{DC-link}}$ $K_i = \frac{{\omega_0}^2 L(\alpha^2-1)}{2V_{DC-link}}$, L and r represent the inductance and its internal resistance, respectively; ω_0 is the angular frequency of the power line; and $\alpha=2\zeta+1$, where ζ is the damping factor.

Its Kp and Ki value is calculated using the Naslin Polynomial method [131]. The output of the PR controller is passed through the DC-link voltage. The output from the DC-link voltage is subtracted from the grid voltage, which is synchronized with the grid phase. Further, it passes through the 1/ DC-link voltage and generates the pulse for switches S_1, S_4, S_3, and S_6.

6.3.4 V2V charging operation

In V2V charging, the energy exchange is implemented by connecting the proposed power processor from both vehicles. For this operation, the power processor restructured itself as a transmitter and the receiver circuit for the energy exchange, and the controller for that is shown in Fig.6. 7(b) and (e). In the energy transmitter vehicle, the controller Fig.6. 7(b) is activated, and the controller parameters are tuned by $\frac{V_{01}}{d_{01}}$ and $\frac{V_{02}}{d_{02}}$ transfer functions. In the energy receiver vehicle, the controller Fig.6. 7(e) is activated, and the controller parameters are tuned by $\frac{V_{accp}}{d_{13}}$ transfer function. The rate of charge is controlled by the microcontroller by fixing the CC-CV value to charge the receiver vehicle.

Table 6. 2 Comparison with similar prior work

		[67]	[35]	[72]	[133]	Proposed
On-board charger		✓	✓	✓	✓	✓
Motoring operation		×	×	✓	✓	✓
V2V charging		×	×	×	✓	✓
V2G power supply		✓	✓	✓	✓	✓
Multioutput		✓	✓	×	×	✓
12 V Auxiliary battery		Required	Required	Required	Required	Not-required
Auxiliary battery charger		Not-required	Not-required	Required	Required	Not-required
Switches	MOSFET, Diode	12,0	11,9	17,0	12,0	13,0
	Additional Switch	4	1	1	3	1
	Total	16	21	18	15	14
Galvanic isolation		✓	✓	✓	✓	✓
Function performs		2	2	3	4	4

6.4 Comparative analysis with similar prior work

The comparison with similar prior work is shown in Table 6. 2. The comparison is represented with the number of functions, the requirement of the auxiliary battery and its charger, the number of switches required, and safety measures. In [67], the integrated converter provides

G2V, V2G and multioutput. However, four additional switches are used for the selection of the function, and the main battery and auxiliary battery cannot be charged simultaneously. In [35], integrated circuit provides G2V, V2G, and multi-output operation and simultaneously charges the main battery and auxiliary battery. However, 21 switches are used for all these operations. Further, an additional converter is required for motoring operations. In [72], the integrated converter provides G2V, V2G, and Motoring operation. However, it cannot charge an additional auxiliary battery. Further, an additional arrangement is required for V2V charging, which is important for mobile charging operations. In [133], the integrated converter provides G2V, V2G, V2V, and motoring operation. However, an additional battery and charger are required for the EV cabin.

The proposed power processor provides G2V, V2G, V2V, and motoring operation with multioutputs to cater to the demand of EV cabins with less number of switches compared to similar prior work.

6.5 Loss analysis of the proposed power processor

The loss analysis is determined by varying the load from 10% to 100% in individual modes of operation. The basic losses, switching loss, diode losses, transformer losses, capacitor equivalent series resistance (ESR) losses, direct current resistance (DC) losses within the inductor, and various other miscellaneous losses, are considered for this analysis.

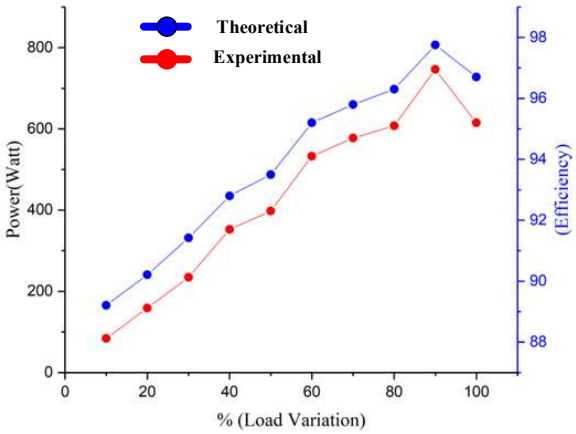

Fig.6. 9 Efficiency curve of G2V operation.

6.5.1 Loss analysis during G2V charging

During the G2V operation, a total of 11 switches are in operation. Switches S_1, S_4, S_3, and S_6 operate at hard switching and provide the PFC. The switches S_7 and S_8 operate at zero voltage

switching (ZVS) with a fixed duty ratio, and these intermediate parts work at the series resonance. Switches S_{11}, S_{12}, and S_{13} provide the multioutput for the cabin power demands. By varying the load from 10% to 100%, the efficiency curve of the proposed converter is given in Fig.6. 9. The peak efficiency of the proposed reversible power processor during G2V operation is 97 %.

6.5.2 Loss analysis during V2G operation

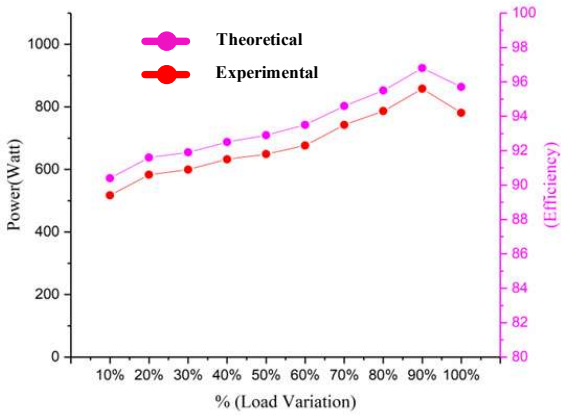

Fig.6. 10 Efficiency curve of V2G operation.

In V2G operation, 11 switches are also operated and provide hard switching. Switches S_9 and S_{10} transfer the power from the battery to the DC link, and it is transferred by switches S_7, S_8, L_r, and C_r through the step-up transformer. The switches S_3, S_4, S_1, and S_6 are controlled according to the grid power requirement. By varying the load from 10% to 100%, the efficiency curve of the proposed converter during V2G power supply is given in Fig.6. 10. The peak efficiency of the proposed reversible power processor during V2G operation is 95.3 %.

6.5.3 Loss analysis during V2V operation

For V2V charging, the proposed power converter from both of the vehicles is directly connected. The high-power auxiliary supply of the multioutput in the energy supplier vehicle is connected with the high-power auxiliary of the energy acceptor vehicle. Therefore, in energy supplier vehicles, S_{11}, S_{12}, and S_{13} are used for the auxiliary power supply and the V2V energy exchange. By varying the load from 10% to 100%, the efficiency curve of the proposed converter during V2V charging is given in Fig.6. 11. The peak efficiency of the proposed reversible power processor during V2V operation is 97.2 %.

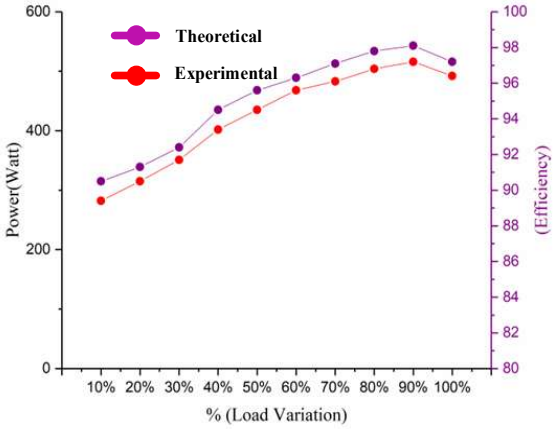

Fig.6. 11 Efficiency of the curve during V2V charging.

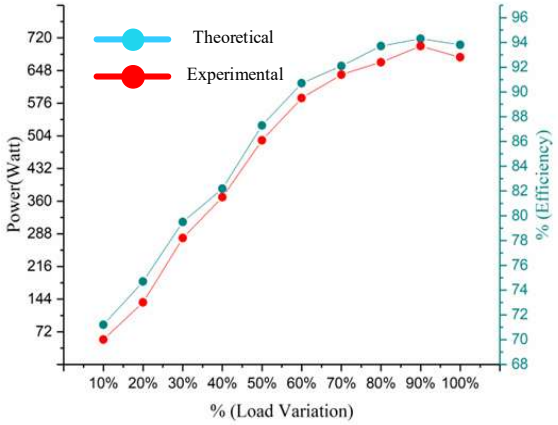

Fig.6. 12 Efficiency curve during motoring mode operation.

6.5.4 Loss analysis during motoring mode operation

In MM operation, 14 switches are also operated and provide hard switching. Switches S_9 and S_{10} transfer the power from the battery to the DC link, and it is transferred by switches S_7, S_8, L_r, and C_r through the step-up transformer. The frequency of switches S_1, S_2, S_3, S_4, S_5, and S_6 is controlled according to the motor's desired speed. By varying the load from 10% to 100%, the efficiency curve of the proposed converter during motoring mode operation is given in Fig.6. 12. The peak efficiency of the proposed reversible power processor during motoring operation is 93.5 %.

6.6 Experimental validation

The photograph of the experimental setup is shown in Fig.6. 13, and the specifications of the selected components are listed in Table 6. 3. The proposed power processor is tested in grid-to-vehicle (G2V) charging, vehicle-to-grid (V2G) power supply, vehicle-to-vehicle (V2V)

charging, and motoring operations. Along with that, auxiliary power supplies are available for all the functions of powering the EV cabin.

Table 6. 3 Specification of the components used in the proposed power processor

Elements	Quantity	Rating
L_{so}	1	2mH
$C_{dc\text{-}link}$	6	470 µF
Transformer	1	740 µH (Lm), 35 µH (Lr), 4:1
Switches	11	650 V, 31 A
Additional Switches	3	450 V, 60 A
Battery	1	48 V, 36 Ah
L_A, L_B	1	1mH, 640 µH
C_{bat}, C_{01}, C_{02}	1	470 µF, 470 µF, 100 µF
Micro-controller	1	TMDSCNCD28335
Induction Motor	1	440 V, 2.5 A

Fig.6. 13 Photograph of the proposed power processor experimental setup.

6.6.1 G2V charging

The proposed power processor maintains the unity power factor at the source terminal, which prevents polluting the grid with harmonics generated by the nonlinear components of the proposed power processor. Also holds the regulated power supply to cater to the power demand of the EV cabin.

6.6.1.1 PFC with auxiliary power supply and THD spectrum of source current

The proposed power processor satisfied the industry standard IEC61000-3-2, which states that the power factor should be less than 0.98 during single-phase charging. The proposed power

processor maintains 0.99 PF at the source terminal, as shown in Fig.6. 14(a). It also satisfied the IEEE 519-2014 standard, where the THD spectrum of source current should be less than 5% during single-phase charging. The proposed power processor maintains the 4.51 % of THD-F at the source terminal, as shown in Fig.6. 14(b).

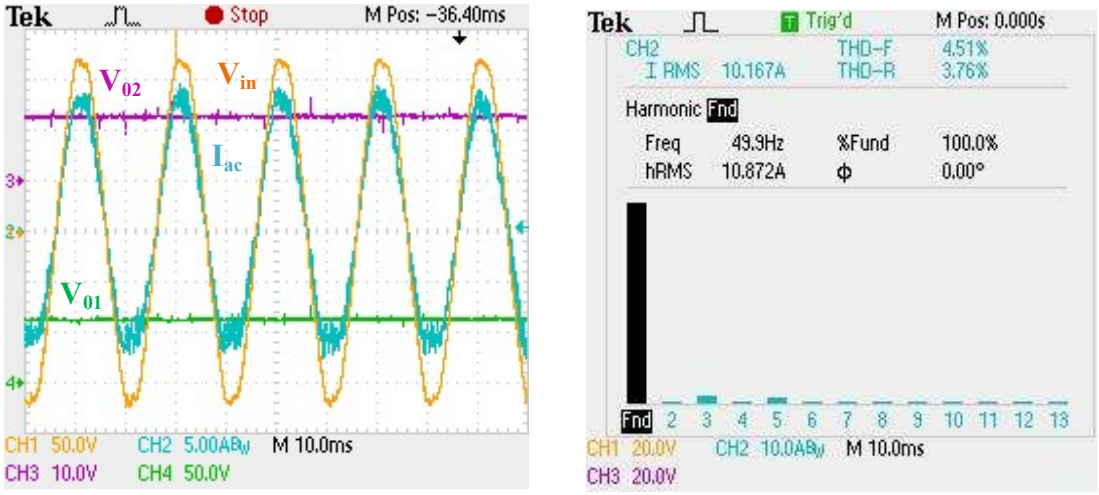

(a) (b)

Fig.6. 14 In charging, (a) PFC with auxiliary power supplies, and (b) THD spectrum of the source current.

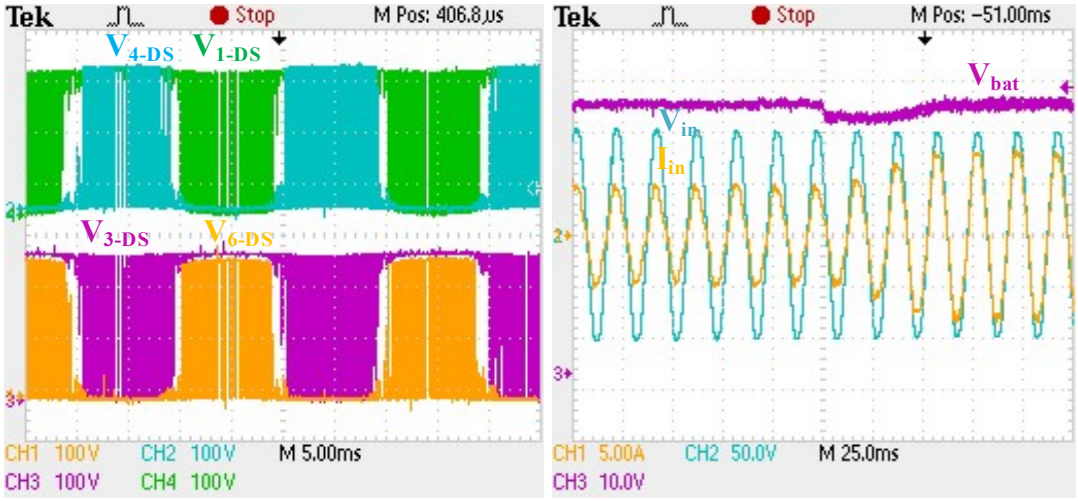

(a) (b)

Fig.6. 15 In charging, (a) voltage across the switch S1, S3, S4 and S6, and (b) PF during load dynamic.

6.6.1.2 PFC switching and load dynamics

For the PFC operation, the controlled signal is simultaneously applied to the switches S_4 and S_6, and it operates according to the positive and negative cycles of the power supply. In the

positive cycle, the supply source switch S_4 is activated, and in the negative cycle, the switch S_6 is activated. According to these, the drain-to-source voltages across the switches S_1, S_4, S_6, and S_7 are shown in Fig.6. 15(a). Further, the proposed power processor maintains the unity power irrespective of the variation of the load. The load dynamic is tested on the variation of resistive load, and its response is shown in Fig.6. 15(b).

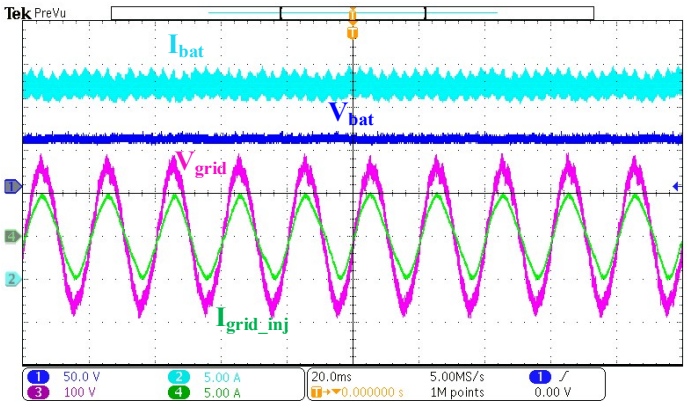

Fig.6. 16 During V2G power supply, the grid voltage (V_{grid}), grid injected current ($I_{grid\text{-}inj}$), battery voltage (V_{bat}), and battery current (I_{bat}).

6.6.2 V2G power supply

A 3.5 A of current is injected into a 120 V bus from the 48 V battery, as shown in Fig.6. 16. During the power transfer, the phase synchronization is an important aspect which is achieved in the proposed power processor.

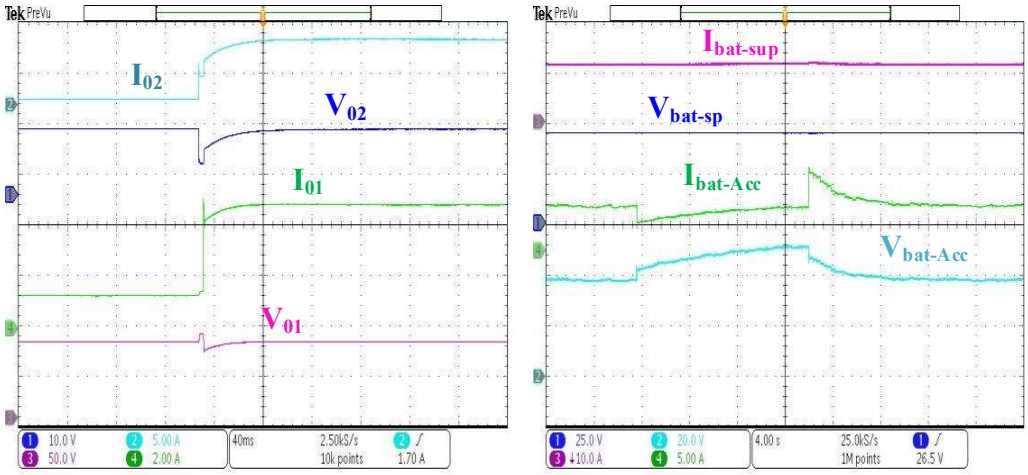

(a) (b)

Fig.6. 17 In V2V charging, (a) load dynamics in the energy supplier vehicle, and (b) load dynamics in the energy acceptor vehicle.

6.6.3 V2V charging

For V2V charging, the proposed power processor from both vehicles is connected. The proposed power processor is restructured and activates the transmitter and receiver circuits according to the energy transfer and the receiver vehicle. The load dynamics are simultaneously applied at the regulated voltages of high-power and low-power auxiliaries as a resistive load, and its stable operation is shown in Fig.6. 17(a). V_{01} and V_{02} are regulated high and low power auxiliary voltages, and I_{01} and I_{02} are the high-power and low-power auxiliary currents.

A CC-CV charging technique is used to charge the acceptor vehicle. A load dynamic is applied in the acceptor vehicle as a resistive load, and the current and voltage profile is shown in Fig.6. 17(b). In the acceptor vehicle, the constant current (CC) is maintained irrespective of the variation of the load. The microcontroller controls the rate of charge of the acceptor vehicle.

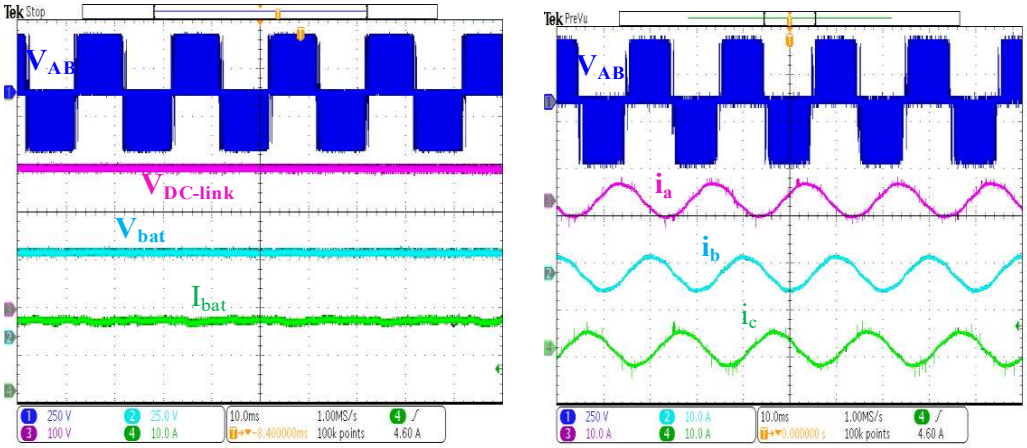

(a) (b)

Fig.6. 18 In motoring mode operation, (a) line voltage V_{AB}, DC-link Voltage, battery voltage, and current, and (b) line voltage with i_a, i_b, and i_c three-phase line current.

6.6.4 Motoring mode operation

In the proposed power processor, a high-voltage induction motor is driven by the 48 V battery. The high voltage is achieved by the step-up transformer, which is used in the charging operation. During the motoring operation, the line voltage V_{AB}, the DC-link voltage, and the battery voltage and current are shown in Fig.6. 18(a). In an electric machine, the current is proportional to the electromagnetic torque. Therefore, the three-phase line current i_a, i_b, and i_c, during the motor drive operation, is shown in Fig.6. 18(b).

6.7 Conclusion

In this chapter, the on-board power processor enables V2G, V2V, and IM drive, operation, and auxiliary power supply in EVs. In this system, all the modes are transferred without any relay, except in motoring mode. A connector "S" is required only in motoring mode operation to connect the motor to the proposed power processor. All the functions are implemented by only 14 switches, which is less compared to similar prior work. The proposed power processor is tested in a load transient condition, and it is found that the system is stable regardless of the variation of the load. A laboratory prototype is tested in 720 W in G2V operation, 1 kW in V2G operation, 490 W in V2V operation, and 768 W in motoring mode operation. Further, the loss analysis is determined in all the modes of operation by varying the load from 10% to 100%. The peak efficiency operation of the proposed power processor in G2V, V2G, V2V, and IM drives is 97%, 95.3%, 97.2%, and 93.5%, respectively.

In the future, the laboratory-scale prototypes will be commercialized as industrial products, and efforts will be made to improve the energy density. Further, the durability may be improved by adding safety measures. Artificial intelligence (AI) will be integrated to monitor performance and detect pre-faults.